THE GEOLOGICAL SOCIETY OF AMERICA®

Cyclostratigraphic calibration of the Eifelian Stage (Middle Devonian, Appalachian Basin, Western New York, USA)

Damien Pas[1,2,†], Anne-Christine Da Silva[2,1], D. Jeffrey Over[3], Carlton E. Brett[4], Lauren Brandt[3], Jin-Si Over[5], Frederik J. Hilgen[6], and Mark J. Dekkers[1]

[1]*Paleomagnetic Laboratory, Utrecht University, Budapestlaan 17, 3584 CD, Utrecht, The Netherlands*
[2]*Pétrologie sédimentaire, B20, Géologie, Université de Liège, Sart Tilman, 4000 Liège, Belgium*
[3]*Department of Geological Sciences, SUNY College at Geneseo, Geneseo, New York 14454, USA*
[4]*Department of Geology, University of Cincinnati, Cincinnati, Ohio 45221-0013, USA*
[5]*Department of Earth and Ocean Sciences, University of Victoria, Victoria, British Columbia, Canada*
[6]*Department of Earth Sciences, Utrecht University, Princetonlaan 8a, 3584 CB Utrecht, The Netherlands*

ABSTRACT

Over the past decade the integration of astrochronology and U/Pb thermal ionization mass spectrometry dating has resulted in major improvements in the Devonian time scale, which allowed for accurate determination of ages and rates of change in this critical interval of Earth history. However, widely different durations have been published for the Middle Devonian Eifelian stage. Here we aim to solve this discrepancy by building an astronomically calibrated time scale using a high-resolution geochemical data set collected in the early to late Eifelian outer-ramp and deep-shelf deposits of the Seneca section (Appalachian Basin, Western New York, USA). The Middle Devonian Eifelian Stage (GTS2012; base at 393.3 ± 1.2 m.y. and duration estimate of 5.6 ± 1.9 m.y.), is bracketed by two major bioevents, respectively the Choteč event at its base and the Kačák event just prior to the Eifelian–Givetian boundary. To capture the record of Milankovitch-scale climatic cycles and to develop a model of the climatic and oceanographic variations that affected the Appalachian Basin during the Eifelian, 750 samples were collected at typically 2.5 cm intervals across the Seneca section. Major and trace elements were measured on each sample with an inductively coupled plasma–optical emission spectrometer. To estimate the duration of the Seneca section sampled, we applied multiple spectral techniques such as harmonic analysis, the multitaper, and evolutionary spectral analysis, and we tuned the Log[10] *Ti* series using the short orbital eccentricity ~100 k.y. cycle. Then, to assess the reliability of our cyclostratigraphic interpretation we ran the Average Spectral Misfit method on selected proxies for detrital input variation. The estimated duration derived using this method falls in the range of durations estimated with the tuning method. Using the approximate position of the Emsian–Eifelian and Eifelian–Givetian boundaries, constrained within <1 m, the proposed estimation of the total duration of the Eifelian age is ~5 m.y. Interpolated from the high-resolution U-Pb radiometric age available for the Tioga F Bentonite, the numerical ages of the Emsian–Eifelian and the Eifelian–Givetian were respectively recalibrated at 393.39 Ma and 388.24 Ma. The uncertainty from the radiometric date is respectively ± 0.86 Ma and ± 0.86 Ma.

INTRODUCTION

In this research we focus on the Middle Devonian Eifelian Age, which was estimated to have a duration of 5.6 ± 1.9 m.y. in the 2012 Geological Time Scale (GTS2012; Becker et al., 2012). The Middle Devonian Epoch is characterized by a relatively high sea level and favorable environmental conditions; it is a key interval in the evolution of life on Earth. Land plants diversified and spread across large areas, which culminated in the development of large trees (Algeo and Scheckler, 1998). The spread of land plants is suspected to have promoted increasing pedogenesis, which triggered continental silicate weathering, leading to increasing CO_2 consumption (Le Hir et al., 2011) and to a notable shift from high to lower atmospheric CO_2 concentrations (Berner, 2006). The high sea level and greenhouse climate also allowed the development of the greatest diversity of marine fauna in the Paleozoic (Sepkoski, 1997) and the concurrent early Middle Devonian fish-tetrapod transition (Niedźwiedzki et al., 2010). The Eifelian is bracketed by two major bioevents, respectively, the Choteč event at the base (House, 1985; Berkyová, 2009) and the Kačák event just prior to the Eifelian–Givetian boundary (Budil, 1995; House, 2002). Both events are characterized by significant physical and biotic turnovers in the marine realm (Chlupáč and Kukal, 1986; House, 2002; Königshof et al., 2016) that include sea-level rise, faunal extinctions, appearance of new life forms, and maximum radiation of goniatites (Walliser, 1986; House, 2002; Vodrážková et al., 2013). Better understanding causes and effects requires a geological time scale as precise as possible. The twofold aims of this study are: (1) to provide a numerical duration constraint for a classic Eifelian section in North America using cyclostratigraphy, and (2) to establish an astronomically calibrated duration for the Eifelian Stage.

Over the past decade, a growing amount of research has been directed toward building an astronomical Devonian time scale with a much higher precision than previous time scales for the Devonian (Ellwood et al., 2011, 2015; De Vleeschouwer et al., 2012, 2013, 2015; Da Silva et al., 2016; Pas et al., 2018). This has led to much better duration estimates for most of the Devonian stages, and, as a corollary, an improved understanding of the timing and causes of Devonian environmental changes (e.g., De Vleeschouwer et al., 2017). The duration estimate for the Eifelian in Becker et al. (2012), i.e., 5.6 ± 1.9 m.y., is based on the cubic spline fit method tied to two high-precision radioisotopic dates from the Tioga F Bentonite (tephra) bed obtained at two widely separated localities from the Appalachian

Damien Pas http://0000-0002-2235-1974
[†]damienpas@gmail.com.

GSA Bulletin; https://doi.org/10.1130/B35589.1; 4 figures; 1 table; 1 supplemental file.

Basin. The first date (389.58 ± 0.86 Ma) was established by Roden et al. (1990) using monazite crystals extracted from the Ziegler pit (Union County, Pennsylvania, USA), and the second (391.4 ± 1.8 Ma) was determined by Tucker et al. (1998) on zircon crystals from Wytheville (Virginia, USA). More recently, De Vleeschouwer and Parnell (2014) integrated astrochronology and Baysian statistics on these same dated zircons and they estimated the duration of the Eifelian Stage at 10 ± 2.7 m.y., which is markedly different. Ellwood et al. (2015) published a cyclostratigraphic calibration of the Eifelian; they proposed a duration of 6.2 m.y. for the Eifelian based on the magnetic susceptibility record of the Bou Tchrafine section in the Tafilalt of SE Morocco.

Needless to say, these very different age estimates of the duration of the Eifelian preclude a complete understanding of the timing and consequences of major biological and paleoceanographic changes occurring at this time. The present study is based on a high-resolution geochemical data set acquired from Seneca County, New York, in eastern North America.

MATERIALS AND METHODS

Litho- and Biostratigraphy of the Sampling Site

During the Eifelian an essentially complete, albeit condensed, succession of outer ramp and deep shelf deposits accumulated within the Appalachian Basin in eastern Laurentia (Ver Straeten, 2007). At that time, the Appalachian Basin was located at ~30°S latitude (e.g., Fig. 1A; Blakey, 2015) within an epieric sea. The Seneca section was sampled in the Seneca Stone Quarry (42°51′22″N, 76°47′8″W) in western New York State, west of Cayuga Lake, in Canoga, Seneca Falls Township, Seneca County, New York. It is an 18.85-m-thick section, encompassing almost the entire Eifelian Stage (i.e., probable *Polygnathus costatus partitus*, *Polygnathus costatus costatus*, *Tortodus kockelianus australis,* and part of the *Tortodus kockelianus kockelianus* zones) consisting of the Onondaga and Union Springs Formations. The following provides a summary of lithostratigraphy; for detailed lithological descriptions of the Onondaga and Union

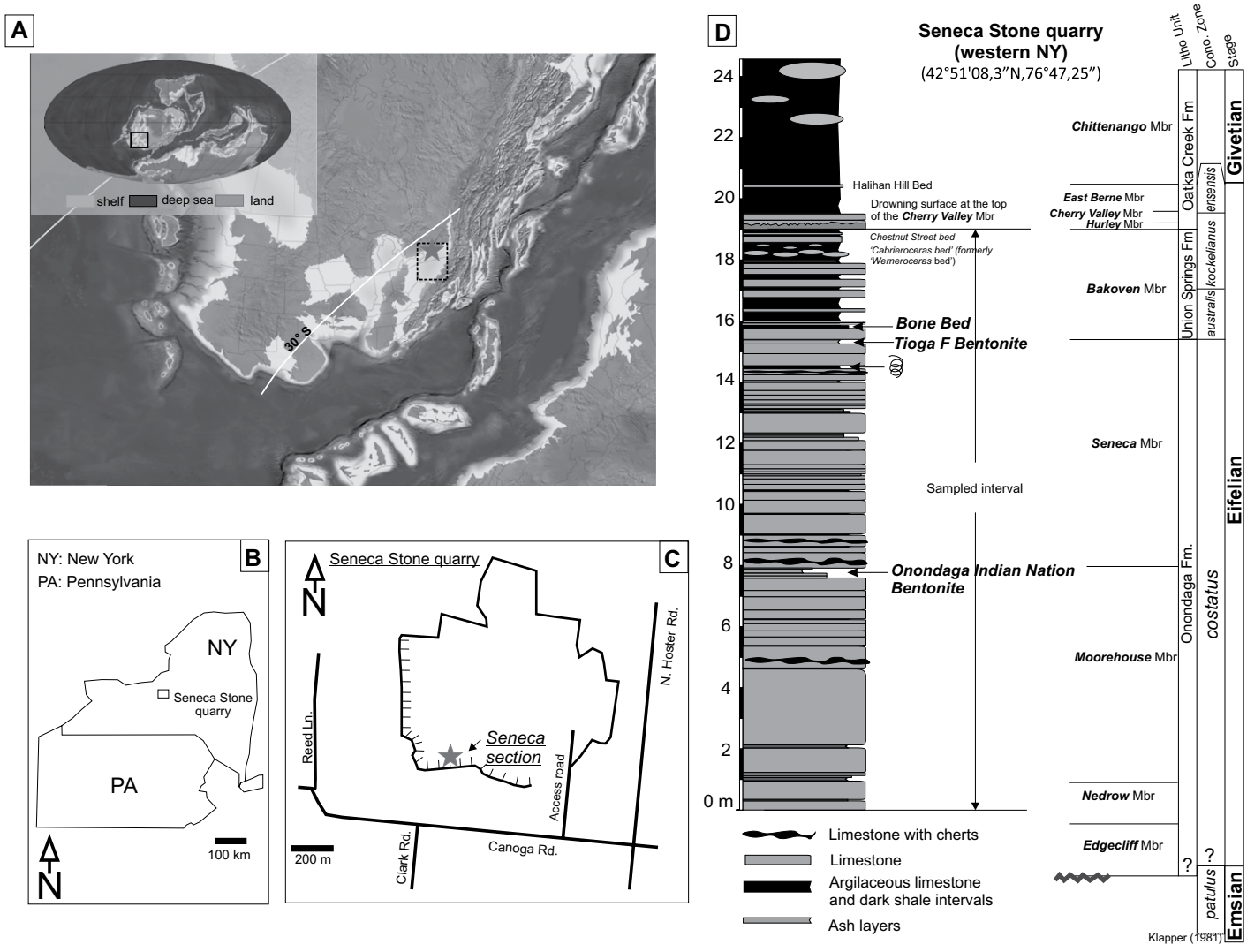

Figure 1. Geological settings of: (A) Location of the Appalachian Basin within the eastern mid-continent of North America, western Laurussia, during the Middle Devonian (Blakey, 2015). Inset shows location of North America in a global paleogeographic reconstruction. (B) Location of the Seneca Stone Quarry in the eastern part of New York State. (C) Location of the Seneca section in the southern wall of the Seneca Stone Quarry. (D) Synthesis log for the Seneca section with lithostratigraphic units and conodont zones, based on Klapper and Ziegler (1979), Ver Straeten (2007), and Brett et al. (2009, 2011). Fm.—formation; Mbr.—member; Cono.—conodont.

Springs Formations, see Ver Straeten (2007). In western and central New York, the Onondaga Formation is subdivided into four members. The basal Edgecliff Member is composed of coarse skeletal grainstone/rudstone typified by large crinoid columnals (~1–2 cm diameter) with a basal biostrome of tabulate and rugose corals and a distinctive 40 cm band of micritic limestone and dark bluish gray chert nodules. The Edgecliff Member has yielded no diagnostic conodonts but has been tentatively identified as belonging to the uppermost Emsian *Polygnathus costatus patulus* Zone based upon bracketing. The underlying Bois Blanc–Schoharie Formation probably belongs to the *Pol. serotinus* Chronozone (based on indirect evidence of icriodid conodonts), whereas the overlying Nedrow Member is arguably of lowest Eifelian *Pol. partitus* Zone, although the precise base of this zone is not established and may lie within the upper portion of the Edgecliff.

The Nedrow Member is the most distinctive interval, ~1.5 m thick, composed of dark gray calcareous shale and argillaceous limestone (lime mudstone) with two decimeter-thick, nearly black shaly beds near the top. The shales are bioturbated with abundant but flattened *Zoophycos* spreiten and thin pyritic burrows. This interval has been correlated with the Choteč event (Ver Straeten, 2007; Brocke et al., 2016). At two localities in central New York the lower part of the Nedrow yielded *Pol. costatus patulus* with *Pol. cooperi cooperi* as well as *Latericriodus latericrescens robustus*, indicative of the *Pol. partitus* Biochronozone, the basal zone of the Eifelian, even though *Pol. partitus* has not itself been identified. The uppermost dark, shaly Nedrow belongs near the base of the *Pol. costatus costatus*, based upon the occurrence of the nominal species at Cherry Valley, New York (Klapper and Ziegler, 1979; Klapper, 1981). The third and thickest member of the Onondaga, the Moorehouse Member, is mainly composed of decimeter-thick sparsely fossiliferous bioturbated wackestone to lime mudstone beds with layers of dark brownish chert nodules. This micritic limestone also shows poorly preserved *Zoophycos* and rare small solitary corals and brachiopods as well as phacopids, odontocephalid trilobites. The entire Moorehouse Member is confidently assigned to the lower part of the *Pol. costatus costatus* Zone based upon the co-occurrence of the nominal conodont with *Pol. costatus patulus* at Cherry Valley, New York (Klapper, 1981). In the middle part of the Onondaga Formation, the Tioga B or Onondaga Indian Nation Bentonite, a yellowish clay bed up to 15 cm thick, forms the boundary between the Moorehouse and Seneca members.

The Seneca Member at the Seneca Stone Quarry (not its type section) is ~17.1 m thick medium dark gray micritic limestone with minor fossiliferous layers, with *Leptaena* and atrypid brachiopods, and scattered dark chert nodules. The entire exposed interval has been unequivocally assigned to the upper part of the *Pol. costatus costatus* Zone based on abundant polygnathid conodonts from across New York State (Klapper and Ziegler, 1979). A distinctive K-bentonite, the so-called Tioga F Bentonite, occurs slightly below the top of the Seneca Member.

The boundary between the Onondaga and Union Springs Formations is defined by the occurrence of a distinctive bone bed that forms a nearly planar contact locally covered with teeth of the sarcopterygian fish Onychodus as well as placoderm armor; this distinctive condensed bone bed, which probably records a major flooding surface, lies ~0.5 m above the Tioga F bentonite layer. Above the bone bed the Bakoven Member of the Union Springs Formation is characterized by 1–10-cm-thick, dark gray argillaceous limestone alternating with organic-rich shale. This interval is very tentatively identified as belonging to the *Tortodus kockelianus australis* Zone, although the nominal species has not been found in New York State. Becker et al. (2012) associated the Bakoven interval as belonging to the *Tortodus k. kockelianus* Zone, although the nominal species is actually found only in the immediately overlying Chestnut Street Bed (Hurley Member; *Wernieroceras* Bed of Klapper, 1981) and Cherry Valley Member of the Oatka Creek Formation. The overlying East Berne Member is argued to be of the *Pol. ensensus* Biochronozone, and the occurrence of the goniatites *Tornoceras* (*T.*) aff. *mesopleuron* (House and Stubblefield, 1965) and an unnamed species of *Parodiceras* near the top of the East Berne in thicker sections in eastern New York indicates the Eifelian–Givetian Stage boundary at about this level (House, 1981; Bartholomew and Schramm, 2013).

Sampling

Seven-hundred-fifty rock samples were collected at ~2.5 cm intervals across the 18.85-m-thick Seneca section at the southern edge of the Seneca Stone Quarry (Fig. 1). The Seneca section interval encompasses almost the entire Eifelian Stage. Based on high-resolution sequence and event stratigraphic correlation of the Seneca section (Brett et al., 2009, 2011) with biostratigraphically dated sections in the Appalachian Basin (Brett et al., 2009, 2011) and our lithostratigraphic data, we infer that the uppermost part of the Eifelian and possibly the lowest part are lacking in the sample collection. Thicknesses of maximum 2 m (though probably much less given that Klapper (1981) regarded most or all of the Edgecliff Member as Emsian) and 1.65 m are respectively missing at the base (i.e., Edgecliff Member) and top of the section (i.e., Hurley, Cherry Valley, East Berne members). Unfortunately, these beds, though well exposed in the Seneca Stone Quarry, were not accessible at the time of sampling. This means that a portion of the *Polygnathus costatus partitus* Zone is missing in the base of the section, and a part of the *Tortodus kockelianus kockelianus* Zone plus the entire *Polygnathus xylus ensensis* Zone are missing at the top of the sampled succession.

Duration estimates for the Eifelian range between extremes of 5.6 m.y. (Becker et al., 2012) and 10 m..y. (De Vleeschouwer and Parnell, 2014). The uncertainty on the estimated duration of the Emsian–Eifelian (i.e., the base of the Eifelian) is 1.2 m.y. according to Becker et al. (2012) and 2.7 m.y. according to De Vleeschouwer and Parnell (2014). The uncertainty on the estimated age of the Eifelian–Givetian boundary (i.e., the top of the Eifelian) is 0.8 Ma according to Becker et al. (2012) and 1.6 Ma according to De Vleeschouwer and Parnell (2014). This leads possible durations of the Eifelian to span between 4.4 m.y. (minimum duration estimate and the corresponding uncertainty [5.6 m.y.–1.2 m.y.]) and 11.6 m.y. (maximum duration estimate and the corresponding uncertainty [10 m.y. + 1.6 m.y.]), which corresponds to sediment accumulation rates (SARs) between 0.16 and 0.42 cm/k.y. with an average at 0.3 cm/k.y. Therefore, the 2.5 cm sampling interval corresponds to ~5.95 k.y. or ~15.6 k.y., respectively. Martinez et al. (2016) established that between 4 and 10 samples per thinnest cycle of interest should preserve spectral peaks of this cycle, but to preserve spectral peaks and significance level a density of 10 samples per putative precession cycle is recommended. Following Martinez et al.'s (2016) recommendations our sampling density should enable meaningful extraction of the long orbital eccentricity and short orbital eccentricity in spectral analysis. The power in the bands of obliquity and precession would likely be low and might not be significant.

Geochemistry

Using an electric drill with a masonry tungsten drill bit, we extracted around 10 gr of fine rock powder per sample for major and trace element measurements. These measurements were performed with an inductively coupled plasma–optical emission spectroscopy (ICP–OES) instrument (Spectro Ciros Vision) at Utrecht University in The Netherlands. Powdered samples were massed with a precision of 0.001 gr and totally dissolved in an aqua regia ($HClO_4$ and HNO_3 mixture)–HF solution for 12–18 h at

90 °C, after which the solution was cooled to room temperature. After this, each solution was diluted to remain within the calibrated concentration range of the ICP–OES instrument. Precision and accuracy of the instrument were both shown to be better than 1% for major elements and 5% for trace elements based on standards from inorganic ventures. In this study, we used the well-known detrital sediment proxies K, Al, K, Ti, Fe, and Cr. All other major and trace element data generated are recorded in Supplemental Material File 1[1]. As a result of the locally high carbonate content versus the very low detrital content in the section, the commonly adopted normalization to Al was not used. Indeed, when concentrations of detrital proxies are very low, sometimes close to zero, ratio values become inconsistent, and the potential trends that might be observed would be a direct artifact of this normalization.

Time-Series Methods

The detection and interpretation of major Milankovitch cycles in the detrital proxy records for the construction of a floating astronomical time scale (ATS) were carried out with Matlab and the signal processing toolbox (see steps 1–8 below). Then, to strengthen and support our astronomical interpretations, we compared our results with the SAR provided by the average spectral misfit technique (ASM, Meyers and Sageman, 2007, steps 9–11). We conducted this latter analysis using the "Astrochron" package developed by Meyers (2014) for the open-source R software platform (http://www.R-project.org/).

The complete protocol for our spectral analysis is as follows (see source of Matlab and R scripts and computer codes in the Supplementary materials):

Tuning Protocol

(1) Data points corresponding to tephra (bentonite) layers were first erased from the data set. The ashes are easily identifiable in the field (soft orange and white sediment) and in the chemostratigraphic profile (Onondaga Indian Nation Bentonite, Tioga F Bentonite, and two other suspected ash beds, Fig. 2).

(2) The data set was then linearly interpolated into an evenly spaced sample record. To better visualize cyclicity in our data set, a log transform was applied to the interpolated record. Minor changes at baseline level are better visualized in log-transformed values as the expression of peak values is attenuated.

(3) The detrital proxy depth series were detrended to remove irregular, very low frequency trends (e.g., linear trend was removed) from the series using *smooth.m* ("loess" option) or *detrend.m.*

(4) To highlight the potential record of astronomically forced sedimentation in the prepared proxy depth series and to detect sediment accumulation rate variations in the depth domain, we generated evolutionary unsmoothed power spectra (or evolutive harmonic analysis, EHA). This was done with the *evofft.m* routine with appropriate sliding windows and the multi-taper method (MTM, Thomson, 1982) calculated using the *pmtm.m.* Adaptive-weighed harmonic F-testing (*mtmdofs.m*, *ftestmtm.m*) was used to estimate the significance level of major wavelengths. The window size is defined based on the sedimentation rates estimated for the studied intervals; it must be large enough to enable meaningful detection of the long and short eccentricity signal. The window must be much smaller than the total data length and must represent 1–1.5× the aimed cycle, i.e., 500 k.y. for a 400 k.y. cycle.

(5) Potential "E" (long orbital eccentricity), "e" (short orbital eccentricity), and "o" (obliquity) cycles representing ~405 k.y., ~100 k.y., and 33 k.y. cycles in the Devonian (Berger et al., 1992) were visually assessed with Taner band-pass filtering (Taner, 2000). This filtering

[1]Supplemental Material. ICP-OES dataset, Matlad and R scripts. Please visit https://doi.org/10.1130/GSAB.S.12284156 to access the supplemental material, and contact editing@geosociety.org with any questions.

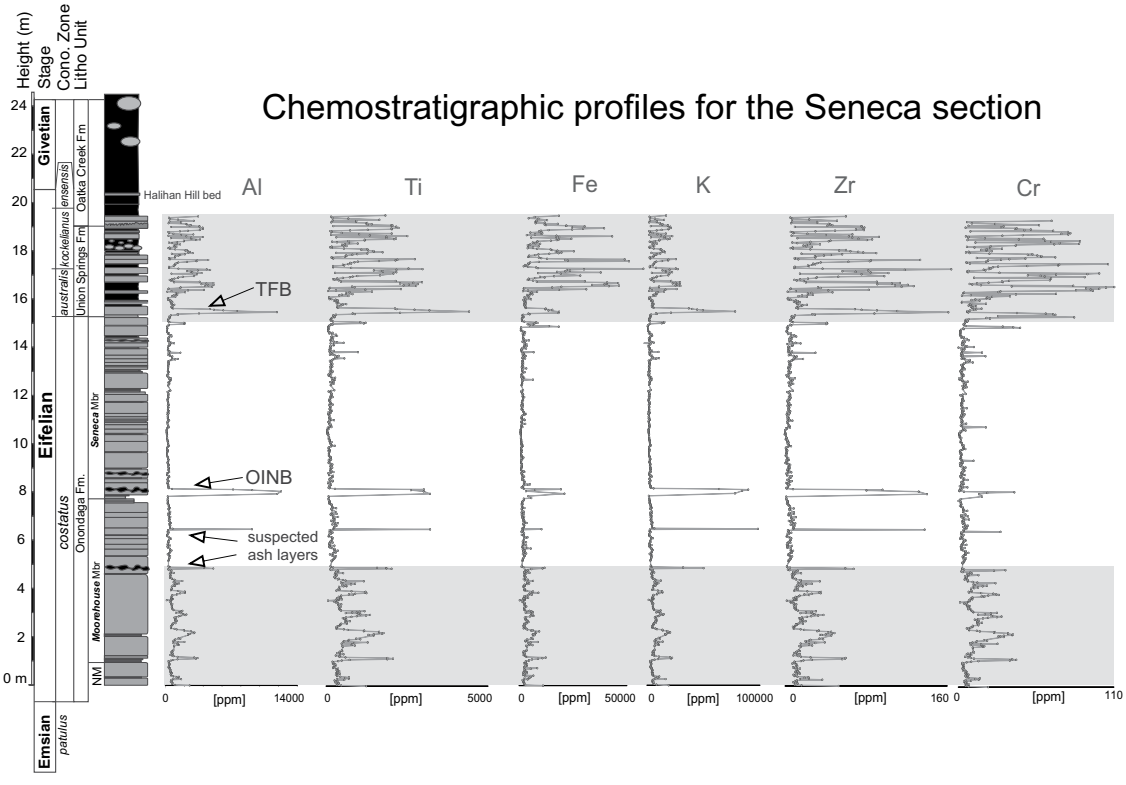

Figure 2. Sedimentological versus chemostratigraphic profiles for the Seneca section. Chemostratigraphic profiles include the elements Al, Ti, Fe, K, Zr, and Cr used as proxies for detrital input delivery into the marine realm for this cyclostratigraphic analysis. Shaded areas are meant to help visualize the three different patterns of detrital proxy variations used within the average spectral misfit protocol to define the three intervals considered to be deposited with steady sediment accumulation rate. All elements are expressed in parts per million (ppm). Arrows pinpoint peaks in Al concentration associated with ash deposits. NM—Nedrow Member; OINB—Onondaga Indian Nation Bentonite; TFB—Tioga F Bentonite; Fm.—formation; Mbr.—member; Cono.—conodont.

was performed with *tanerfilter.m* and allowed accurate isolation of the cycles in the stratigraphic domain (a constant sedimentation rate is assumed). Based on the interpreted "E," "e," and "o" cycles, we carried out a "minimal tuning with linear interpolation" (Muller and MacDonald, 2000) using *depthtotime.m*. Minimal tuning is the practice of tuning to a single astronomical frequency, which should result in the alignment of other astronomical frequencies. In this study, the 100 k.y. short orbital eccentricity cycle was used for tuning.

(6) The resulting time-series were resampled with an appropriate uniform Δt based on the original sample rates.

(7) Evolutionary power spectra and the MTM spectral analysis with harmonic F-testing as in Step 2 were applied to the newly constructed time series.

(8) The high-resolution floating ATS was associated with the rather well-constrained conodont biostratigraphic framework.

Average Spectral Misfit Protocol

(9) Prior to running the ASM we first prepared our proxy data (Ti, Al, Cr, Fe, Zr, and K) using similar procedures as in Matlab (e.g., steps 1–3 above) but performed in R (e.g., removing data points corresponding to bentonite layers and running a linear interpretation and log transformation).

(10) By combining results from evolutionary unsmoothed power spectra and field observation (e.g., lithology), the Seneca section was divided into three intervals of relatively stable SAR. For each of these intervals, we subsequently performed MTM analysis and the corresponding adaptative harmonic F-testing. Frequencies equal to or higher than the 95% confidence level in both analyses were extracted. These frequencies were implemented into the ASM command. The ASM technique, developed by Meyers and Sageman (2007), measures the distance between the frequencies obtained through spectral analysis with the theoretical orbital frequencies and computes the SAR that provides the best fit with the highest confidence level. Each ASM run includes an unequivocal statistical test for rejection of the null hypothesis of no orbital forcing (Ho_SL). The target frequencies for the Eifelian used in ASM runs are based on Berger et al. (1992), and they correspond to periodicity of the long- and short-orbital eccentricities (1/405.75 k.y., 1/126.98 k.y., and 1/96.91 k.y.), the obliquities (1/39.1 k.y. and 1/31.86 k.y.), and the precessions (1/19.8 k.y. and 1/16.8 k.y.). In this analysis, ASM runs that do not generate a fit with each target frequency (e.g., astrofit <7) are discarded in step 11.

(11) Based on calculated SARs (expressed in cm/kyr, obtained with ASM) for each proxy and thicknesses (expressed in cm), we calculated durations for each interval. Then, by adding the duration of each interval, we calculated the duration of the whole Seneca section. These durations were then compared with the duration obtained through the minimal tuning (steps 1–8).

RESULTS AND DISCUSSION

Origin of Geochemical Variations

Variations in major and trace elements such as Ti, Al, Fe, K, Cr, and Zr in marine sequences are usually associated with changes in concentration of siliciclastic materials triggered by the erosion of continental rocks. These elements are considered reliable proxies for detrital input (Calvert and Pedersen, 2007) and are commonly used as proxies for paleoclimate reconstruction (Calvert and Pedersen, 2007; Sinnesael et al., 2017). For instance, an increase in the concentration of these elemental proxies in a marine sequence is usually interpreted as a higher rate of runoff, which can be triggered by an increasing hydrological regime (e.g., more intense rainfall or sea-level drop). Variations in detrital input proxies can therefore be attributed to different causes, depending on the time scale involved.

Changes in summer insolation driven by the Milankovitch precession cycles play a crucial role in the intensity and amount of precipitation and wind. This precipitation variation results in substantial changes in riverine or eolian input into the global oceanographic system, which in turn affect the concentration in detrital materials accumulated in the sedimentary archives. The imprint of orbitally controlled detrital variation in Paleozoic sedimentary successions has been observed in various paleogeographic settings. It enables construction of high-resolution time scales and reconstruction of the paleoclimatic history for multiple time intervals of interest (e.g., De Vleeschouwer et al., 2017; Pas et al., 2018; Wu et al., 2019). The outer ramp and deep shelf depositional setting recorded at the Seneca Stone Quarry, together with the subtropical paleolatitude, made the record in this quarry a very good candidate for detecting a preserved Milankovitch-forced climate.

Cyclostratigraphy

Trends and variations within the main detrital proxies recorded through the Seneca section are highly similar (Fig. 2) and likely driven by similar factors. Based on the visual evaluation of Ti, Al, K, Zr, and spectrograms, we chose Ti as a reference proxy to conduct the complete Matlab time-series protocol because peaks of interest clearly stand out. The power spectrum of the untuned Seneca section Ti depth series shows prominent sedimentary cycles at wavelengths of ~1.85 m and ~0.43 m and weaker peaks in the range of 0.15 m and 0.1 m (Fig. 3B). The evolutionary fast Fourier transform (FFT) spectrogram shows a slight shift in all peaks at the same depth, which indicates a slight variation of SAR (Fig. 3D) As mentioned in the sampling procedure, the SAR in the Seneca section can range from 0.16 cm/k.y. to 0.42 cm/k.y. (Becker et al., 2012; De Vleeschouwer and Parnell, 2014), and the average SAR is 0.3 cm/k.y. The ratio of the wavelengths 2.9–1.8 m, 0.74–0.34 m, 0.16–0.12 m, is ~12:4:1, which is consistent with the expected ratio for long-term orbital eccentricity (~405 k.y.), short-term orbital eccentricity (~100 k.y.), and obliquity (~33 k.y.) in the Devonian (Berger et al., 1992). Based on our interpretation of prominent peaks in the Log^{10} *Ti* series spectrogram (Fig. 3), the SARs are between 0.5 cm/k.y. and 0.4 cm/k.y., which are close to the SAR calculated from the Eifelian duration of Becker et al. (2012). Interpreted 405 k.y. and 100 k.y. cycles in the Log^{10} *Ti* series were band-pass filtered using the 2.9–1.3 m and the 0.74–0.34 m wavelengths (Fig. 3A) that respectively correspond to frequency ranges 0.34–0.77 m^{-1} and 1.35–2.9 m^{-1}. We used the 100 k.y. orbital eccentricity cycle for the tuning of the Log^{10} *Ti* series, and based on the 100 k.y. filter output we assigned 42 short-term orbital eccentricity cycles through the Seneca section studied (i.e., almost the entire Onondaga Formation and the Union Springs Formation). The interpreted long-term orbital eccentricity was also filtered out, and when plotted against the 100 k.y. short orbital eccentricity, it shows a relatively clear amplitude modulation of the 405 cycles through most of the Seneca section (Fig. 3B). The power spectrum of the 100 k.y.-tuned record of the Seneca section Log^{10} *Ti* series (Fig. 4B) shows significant peaks in the frequency range of eccentricity (405 k.y. and 100 k.y. (tuned)) and several high-amplitude peaks in the range of obliquity (33 k.y.). The split of the obliquity period into three main peaks was expected as we tuned using a single 100 k.y. cycle (e.g., Yao et al., 2015). Indeed, during the 100 k.y. tuning we assigned a sedimentation rate for each 100 k.y. interval, although the obliquity forcing recorded in sedimentary sequences is prompted or responding to another sedimentation rate. The evolutionary FFT spectrogram indicates a stable 405 k.y., a good alignment with the 100 k.y. eccentricity term, and sporadic higher power in the band of obliquity. Even though the 405 k.y. cycle dominates the deposition in the Seneca section, a shift from long orbital to short orbital eccentricity is expressed in the upper portion of the evolutionary FFT diagram for the tuned Seneca section

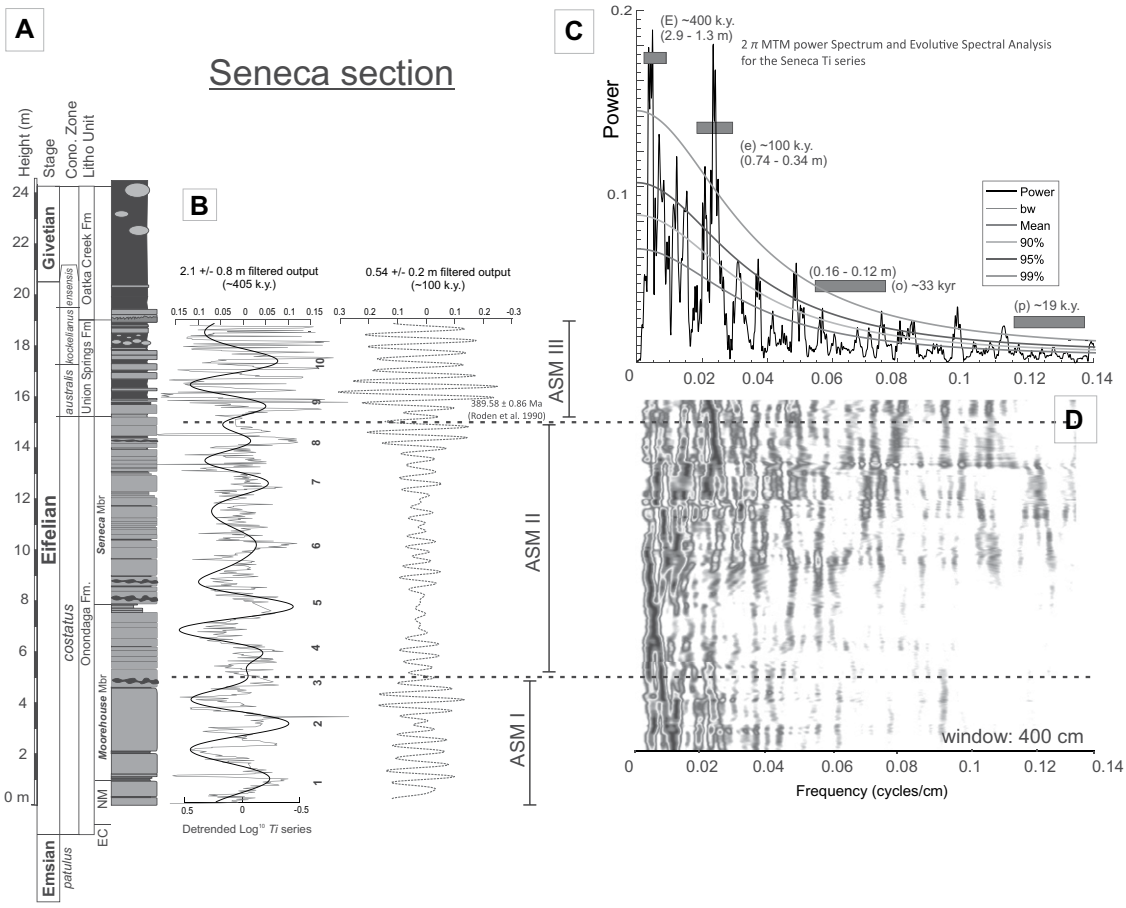

Figure 3. Biostratigraphy, lithology, detrended Log[10] *Ti* curve, and band pass filters of the log[10] *Ti* series for the Eifelian interval in the Seneca section. Biostratigraphy is based on the combined data from Klapper and Ziegler (1979) and summarized in Brett et al. (2009, 2011). (A) Lithological units as defined for the Seneca Stone Quarry with corresponding conodont zones and lithology observed in the Seneca section. (B) Detrended Log[10] of *Ti* series against the ~405 k.y. and ~100 k.y. filtered output extracted with Taner band pass filtering using lower and upper cut off values as presented in Figure 3C spectral power. (C) The 2π multitaper method (MTM) power spectrum of the detrended Log[10] of *Ti* series showing distribution of the spectral power in the stratigraphic domain. The lowest frequency band, in a frequency range of 0.34–0.77 m^{-1} (2.9–1.3 m), is interpreted as the result of an ~405-k.y.-long orbital forcing cycle (E in part C). The low frequency bands in the range of 1.35–2.9 m^{-1} (0.74–0.34 m) and 6.2–8.3 m^{-1} (0.16–0.12 m) are respectively interpreted as the 100 k.y. short orbital eccentricity (e) and the ~33 k.y. obliquity (o) forcing. (D) Evolutive fast Fourier transform (FFT) spectrogram for the detrended Log[10] of *Ti* series using a 400 cm (4 m) window. The three main frequency bands characterized by peaks in spectral power can be observed in the FFT spectrogram with some discontinuities that are likely the results of changes in the sedimentation accumulation rate (SAR). Average spectral misfit (ASM) I to ASM III on the left side of the evolutive FFT spectrogram correspond to the intervals of considered constant SAR selected for running the ASM function. NM—Nedrow Member, EC—Edgecliff Member.

Log[10] *Ti* series. The SAR calculated for each 100 k.y. interval through the Seneca section fluctuates from 0.1 to 0.9 cm/k.y. with an average of 0.4 cm/k.y. The duration of the Seneca section Log[10] *Ti* series based on the short orbital eccentricity tuning is 4.2 m.y.

To assess the reliability of our cyclostratigraphic interpretations we ran the Average Spectral Misfit method on our detrital proxy data and extracted the SAR separately on the three intervals taken to record constant SAR because of similar lithological features (ASM I, ASM II, and ASM III, Fig. 3). These intervals appear to be well distinguished in the chemostratigraphic profiles of Ti, Al, Fe, Cr, K, and Zr (Fig. 2), all of which follow similar trends. The first interval (ASM-I) extends over the first 5 m, starting at the base of the section and ends just above a cherty bed associated with the lowest geochemically identified ash layer (see Fig. 2). This interval belongs to the Nedrow and lower Moorehouse members and shows oscillations in all the detrital proxies. The second interval (ASM II) extends from 5 m to 15 m and covers the upper portion of the Moorehouse Member and the entire Seneca Member. This interval includes two important K bentonite (tephra) layers, respectively, the Onondaga Indian Nation Bentonite (at ~8 m stratigraphic level in the section) and the Tioga F Bentonite (at ~15 m). The latter coincides with the upper boundary of interval ASM II. Geochemical variations throughout ASM II are relatively low in amplitude compared to intervals I and III. The third interval (ASM III, Fig. 3), which belongs to the Union Springs Formation, starts just above the Tioga F Bentonite at 15 m stratigraphic level and ends at the end of our record at 18.85 m. Interval III records very high amplitude variations in all detrital proxies as well as other analyzed elements such as Ca. At the outcrop scale, these variations are expressed by an alternation from thin-bedded limestone to dark, organic-rich siliciclastic beds.

MTM and ASM analyses were conducted on each of the three intervals utilizing the six prepared (e.g., step 9) detrital proxy values (Ti, Al, Zr, Fe, Cr, and K) as summarized in Table 1. Before initiating the ASM function, the possible SAR range must be defined. Based on available biostratigraphic data (Klapper and Ziegler, 1979; Brett et al., 2009, 2011), we know that the uppermost and lowermost part of the Eifelian in the sampled Seneca section is lacking in the sample record. To account for the short intervals

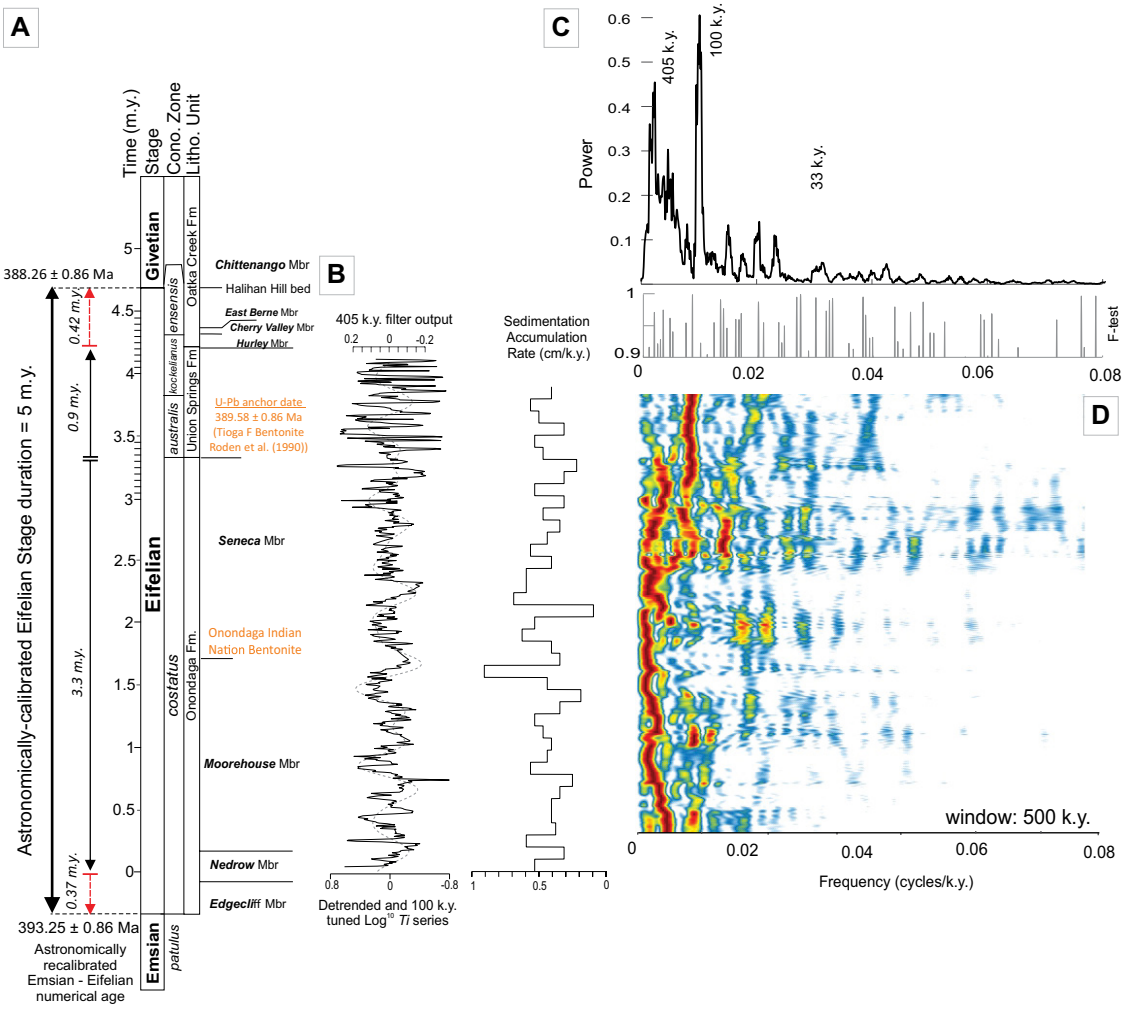

Figure 4. Spectral analysis of the Seneca section detrended Log[10] of *Ti* series after tuning to time domain. (A) Astronomically calibrated duration for the Eifelian Stage and corresponding astronomical time scale (ATS), lithological units, and conodont zones as defined for the Seneca section. The red dashed arrows in the lower and upper limits of the floating ATS indicate extrapolated durations for the missing uppermost and lowermost Eifelian in the section. (B) Detrended 100 k.y. tuned Log[10] *Ti* series with 400 k.y. filtered curve and Sediment Accumulation Rate curve showing the average values for each 100 k.y. cycle identified for tuning. (C) The 2 π multi-taper method (MTM) spectral plot shows the strong tuned, 100 k.y., short orbital eccentricity peak and one prominent peak at 405 k.y. with reliable F-test below. Power in the band of obliquity (33 k.y.) is low. (D) Evolutive fast Fourier transform (FFT) spectrogram for the Seneca section shows strong and stable power in the 405 k.y. orbital eccentricity periodicities band and discontinuity in the 100 k.y. orbital eccentricity periodicities band (window observation is 500 k.y. and step rate is 3.5 k.y.). Mbr.—member; Cono.—conodont.

of missing Eifelian deposits/time (i.e., those not included in the ASM intervals) and/or larger changes in SAR variations, we chose a range of SAR extending from 0.01 to 1.5 cm/k.y. For the ASM I interval (0–5 m), MTM and ASM show consistent results for all six elements. For the first interval, average SARs vary between 0.32 cm/ky and 0.54 cm/k.y., depending on the element considered, with Ho_SL values between 0.4 and 8.3, which indicates there is between 0.4% and 8.3% probability that ASM results are produced by chance. In this interpretation, the prominent low frequency power band observed at 0.0048 cm^{-1} (or at a period of 200 cm) in the upper part of the EHA (Fig. 3A) can be linked with the 405-k.y.-long orbital eccentricity. Accounting for the thickness and the calculated range of average SAR, the duration of the first interval, ASM I, is between 925 k.y. and 1562 k.y. In the ASM II interval, SAR values are between 0.51 cm/k.y. and 0.66 cm/k.y. and Ho_SLs for the six elements considered are all lower than 4.7. The SAR between 0.51 cm/k.y. and 0.66 cm/k.y. can be attributed to a 405 k.y. cycle with a period of 2.43 m (frequency of 0.0041 cm^{-1}). Based on the thickness and range of SAR durations, this interval would last between 1515 k.y. and 1960 k.y. In the ASM III interval (15–18.85 m), the SAR values vary between 0.34 cm/k.y. and 0.42 cm/kyr. Ho_SL values are low for Al, Ti, Fe, and K (ranging between 2.58 and 5.6) and relatively high for Zr and Cr (21 and 23.47), discrediting these latter two elements. Additionally, ASM results for Fe, Cr, and Zr proxies indicate that major frequencies for these elements do not match all seven astronomical targets defined in step 10 of the ASM protocol (e.g., astrofit values <7 for Cr, Fe, and Zr; see Table 1). ASM runs for Al, Ti, Fe, and K proxies indicate a fit with the seven defined astronomical targets. With these interpretations, the low frequency power band observed at 0.0063 cm^{-1} (or at a period of 157 cm) can be correlated with the 405-k.y.-long eccentricity cycle. Duration for the ASM III interval, therefore, ranges between 897 k.y. and 1117 k.y. Accounting for all three intervals, the shortest and longest duration estimates of the Seneca section, calculated using the ASM method, are between 3.3 m.y. and 4.6 m.y., which is well within the range of the duration estimate of 4.2 m.y. obtained by the minimal tuning method.

Cyclostratigraphic Calibration for the Eifelian Time Scale

Based on the astronomical tuning we can construct a floating ATS for the Eifelian. From an astronomical point of view, the 405 k.y. long-term orbital eccentricity cycle provides a reliable geochronometer for tuning long sedimentary records because it is caused by the gravitational interaction of Jupiter and Venus, the former of which has an extremely stable orbit (Olsen,

TABLE 1. SYNTHESIS OF AVERAGE SPECTRAL MISFIT (ASM) TECHNIQUE RUNS CARRIED OUT FOR THE SELECTED DETRITAL PROXIES ON THE THREE DIFFERENT INTERVALS CONSIDERED TO BE DEPOSITED WITH CONSTANT SEDIMENT ACCUMULATION RATE (SAR)

ASM interval	Ho-SL	AstroFit (<7)	SAR (cm/kyr)	Duration (kyr)
ASM-I (0–5 m)				
Al	0.715		0.5451	917.26
Cr	0.636		0.5451	917.26
Fe	7.6		0.3286	1521.61
K	0.44		0.54	925.92
Ti	7.7		0.3636	1375.14
Zr	8.3		0.3824	1307.53
ASM-II (5–15 m)				
Al	4.651		0.6674	1498.35
Cr	4.198		0.6344	1576.30
Fe	2.3		0.5181	1930.13
K	4.025		0.49	2040.82
Ti	3.5		0.6344	1576.29
Zr	3.2		0.634	1577.29
ASM-III (15–18.85 m)				
Al	4.404		0.4232	897.92
Cr	21	3	0.103	3689.32
Fe	2.58	4	0.19	2000.00
K	4.28		0.34	1117.64
Ti	5.6		0.4232	897.921
Zr	23.47	3	0.103	3689.32

Notes: (SAR, see Fig. 3). The ASM function is performed with the astrochron package (Meyers and Sageman, 2007) in the open-source software R. Ho-SL—Null hypothesis significance level (0–100 percent). Astrofit—Number of astronomical terms fit.

2001; Laskar et al., 2011). In this study, several parameters led us to tune the Seneca section *Ti* series using the 100 k.y., short-term orbital eccentricity cycle. Indeed, the sedimentary record under investigation represents a relatively short time interval, recording a limited number of 405 k.y. cycles (i.e., the cycle commonly used for tuning long records in the Paleozoic), which lowers the statistical relevance and accuracy of the tuning. The amplitude modulation of short-term eccentricity cycles by the 405 k.y. cycle (Fig. 3), however, indicates a good recording of both astronomical cycles in the stratigraphic series, which supports the tuning with the 100 k.y. cycles. Additionally, tuning to the short orbital eccentricity allows the development of a floating ATS of 4.2 Ma with a 100 k.y. precision for the Seneca section.

Lower and Upper Eifelian Boundaries in the Seneca Section

Based on the Devonian biostratigraphy of Klapper and Ziegler (1979) and Klapper (1981) in the Appalachian Basin and our lithostratigraphic data, it appears that the base of the Seneca section belongs to the lowermost part of the Eifelian (e.g., base of *Pol. costatus partitus* Zone) and the Emsian–Eifelian boundary is located in, or at the base of, the Edgecliff Member (see Klapper and Ziegler, 1979; Brett et al., 2009) at a maximum of 2 m down the section (i.e., considering the base of the Edgecliff Member as the Emsian–Eifelian boundary). Given the relatively similar lithology throughout the Nedrow and Edgecliff members, we assumed that the calculated sediment accumulation rate at the bottom of the section (e.g., 0.54 cm/k.y.; see Fig. 4) can be extrapolated, which would account for 370 k.y. [200 cm/0.54 cm/k.y.]. The uppermost portion of the stratigraphic interval studied belongs to the upper part of the *Tortodus kockelianus* conodont zone (e.g., latest Eifelian). The upper *T. kockelianus kockelianus* and *Polygnathus xylus ensensis* zones (the uppermost Eifelian conodont zone), corresponding to the Cherry Valley and East Berne members, were not sampled. Based on our measurements, 1.65 m of dark gray shale separates our last sample (i.e., 18.85 m) from the Eifelian–Givetian boundary, which is located approximately at the base of the fossiliferous Halihan Hill Bed at 20.5 m (see Fig. 1D). Given the homogeneous lithology characterizing the uppermost Eifelian, it is safe to extrapolate the SAR calculated for the uppermost part of the section (0.4 cm/k.y., see Fig. 4). Based on those assumptions, the time missing in the uppermost part of the section would be 420 k.y. [165 cm/0.4 cm/k.y.].

Following the step-by-step time series protocol defined in Matlab, which includes analyses in both stratigraphic and time domains (e.g., Sinnesael et al., 2019), we were able to construct an astronomically calibrated time scale for the Seneca section Log^{10} *Ti* series, which covers most of the Eifelian. The Seneca section duration based on the 100 k.y. minimal tuning is estimated at 4.2 m.y. To strengthen/support this duration estimate we conducted independent analyses with the ASM method (Meyers and Sageman, 2007) on six detrital proxies. The calculated duration estimates for the Seneca section using ASM range between 3.3 m.y. and 4.6 m.y., which indicate a relatively small degree of uncertainty in the estimate obtained with minimal tuning.

Accounting for the calculated time for the missing lower and upper parts, the Eifelian Stage is estimated at 4.2 m.y. + 0.8 m.y. = 5 m.y., which is comparable to the radiometrically constrained duration of the Eifelian established in Becker et al. (2012) but significantly shorter than the duration of 10 m.y. estimated in De Vleeschouwer and Parnell (2014). In De Vleeschouwer and Parnell (2014), estimate durations were calculated by incorporating available Devonian astrochronologies (Frasnian, Givetian, and Upper Famennian) and high-precision radiometric dates (i.e., D0 to D18 in Becker et al., 2012) in a Baysian-based statistical model (i.e., Bchron model). Incorporation of the Givetian, Frasnian, and upper Famennian astrochronologies in the Bchron model has significantly reduced the uncertainties of these time intervals. However, as the model is constrained by the Silurian–Devonian and Devonian–Carboniferous numerical radiometric dates, the reduction of uncertainties and times for one or another interval strongly impacts the other "less constrained" intervals and their respective boundaries, where one can observe an important increase in the uncertainties and duration compared to Becker et al.'s (2012) time scale, for instance. So, it is suggested that the significantly longer estimated duration defined in De Vleeschouwer and Parnell (2014) results from an error propagation in the fewer time constraints available (i.e., high-precision U-Pb dates) and that the newly constructed, independent astronomically calibrated time scale in this study should be used for Devonian time scale calibration. By summing the high-precision numerical date of the Tioga F Bentonite (389.58 ± 0.86 Ma; Roden et al., 1990), the duration estimated for the interval that separates the Tioga F Bentonite and the lower Eifelian boundary (i.e., 3.3 m.y., see Fig. 4A) and the extrapolated duration for the missing lowermost Eifelian, we obtained a new estimate of the numerical age of the Emsian–Eifelian boundary ([389.58 Ma] + [3.3 m.y. + 0.37 m.y.] = [393.25 Ma]). Following a similar approach, the new numerical age for the Eifelian–Givetian boundary is estimated at 388.26 Ma ([389.58]–[0.9 m.y. + 0.42 m.y.]). Uncertainties extrapolated from the radiometric date on the Emsian–Eifelian and Eifelian–Givetian boundaries are respectively ± 0.86 Ma and ± 0.86 Ma. As largely discussed in Sinnesael et al. (2019), estimation of uncertainties in cyclostratigraphy is relatively complex, and they encourage researchers to provide the source of uncertainties rather than an arbitrary number of cycles as an uncertainty estimate. In

this study, the following sources of uncertainties were identified:

(1) Stratigraphic errors can arise from the position of the Emsian–Eifelian and Eifelian–Givetian stage boundaries (see section on lower and upper Eifelian boundaries in the Seneca section);

(2) Errors can arise from the point that was set as the starting point for counting the 100 k.y. short eccentricity cycle in the tuning procedure. This point is arbitrary and can correspond to any point between two minima/maxima;

(3) Errors could arise from erasing data points that correspond to ash layers. After erasing those data points, we generated artificial data points (e.g., linear interpolation) and therefore created an artificial signal from which errors can arise.

(4) Finally, there are some uncertainties between results obtained by tuning and those obtained by ASM on the different proxies.

CONCLUSIONS

The Seneca section in west central New York State provides a high-resolution record of the early to late Eifelian in the Appalachian Basin, which represents the most complete outer-ramp and deep-shelf record of this time frame yet described. Time series analysis of the $\log^{10}$ *Ti* data set from this section highlights significant sedimentary cycles, which were successfully attributed to astronomically forced Milankovitch cycles. Minimal tuning with the short-term orbital eccentricity allowed a precise estimate of the duration of the Seneca section at 4.2 m.y. The reliability of this tuning was assessed through the Average Spectral Misfit method on selected detrital proxies. The estimated duration derived from the tuning falls in the range of durations estimated with the ASM method, strongly supporting our interpretations. Using the approximate position of the Emsian–Eifelian and Eifelian–Givetian boundaries constrained within <1 m, it permits an estimate of the total duration of the Eifelian Stage at 5 m.y. Using the U-Pb anchor date from the Tioga F Bentonite, the numerical age of Emsian–Eifelian and the Eifelian–Givetian were respectively recalibrated at 393.25 Ma and 388.26 Ma. The uncertainty from the radiometric date is respectively ± 0.86 Ma and ± 0.86 Ma. Sources of uncertainties that arise from the astronomical tuning protocol were also identified, such as the linear interpolation, the stratigraphic position of the Emsian–Eifelian and Eifelian–Givetian stage boundaries, and the creation of artificial data points replacing those erased from the ash layers, as well as small differences between the different spectral techniques.

ACKNOWLEDGMENTS

This work is supported by Netherlands Organization for Scientific Research (NWO, grant WE.210012.1). Anne-Christine Da Silva acknowledges FNRS grant PDR T.0051.19. This research would not have been possible without the cooperation of the Seneca Stone Quarry, which kindly provided access and permission to sample the section. We thank Editor Brad Singer, Associate Editor Bradley D. Cramer, and two anonymous reviewers for their thorough reading and constructive comments that helped to improve this manuscript. This paper is a contribution to International Geoscience Programme 652: Reading Geologic Time in Paleozoic Sedimentary Rocks. Published with the support of the Belgian University Foundation.

REFERENCES CITED

Algeo, J.T., and Scheckler, S.E., 1998, Terrestrial–marine teleconnections in the Devonian: Links between the evolution of land plants, weathering processes and marine anoxic events: Philosophical Transactions of the Royal Society of London, v. 353, p. 113–130, https://doi.org/10.1098/rstb.1998.0195.

Bartholomew, A.J., and Schramm, T.J., 2013, The nature and timing of the Middle Devonian Kačák bioevents in the Marcellus Subgroup of the Appalachian Basin: Palaios, v. 28, no. 11, p. 825–836.

Becker, R.T., Gradstein, F.M., and Hammer, Ø., 2012, Chapter 22—The Devonian Period, *in* Gradstein, F.M., Ogg, J.G., Schmitz, M.D., and Ogg, G.M., The Geologic Time Scale, v. 1–2, p. 559–601, https://doi.org/10.1016/B978-0-444-59425-9.00022-6.

Berger, A., Loutre, M.F., and Laskar, J., 1992, Stability of the astronomical frequencies over the Earth's history for paleoclimate studies: Science, v. 255, no. 5044, p. 560–566, https://doi.org/10.1126/science.255.5044.560.

Berkyová, S., 2009, Lower–Middle Devonian (upper Emsian–Eifelian, serotinus–kockelianus zones) conodont faunas from the Prague Basin, the Czech Republic: Bulletin of Geosciences, v. 84, no. 4, p. 667–686, https://doi.org/10.3140/bull.geosci.1153.

Berner, R.A., 2006, GEOCARBSULF: A combined model for Phanerozoic atmospheric O_2 and CO_2: Geochimica et Cosmochimica Acta, v. 70, no. 23, p. 5653–5664.

Blakey, R., 2015, Colorado Plateau Geosystems, Volume 2015.

Brett, C.E., Ivany, L.C., Bartholomew, A.J., DeSantis, M.K., and Baird, G.C., 2009, Devonian ecological-evolutionary subunits in the Appalachian Basin, *in* Königshof, P., Devonian Change: Case Studies in Palaeogeography and Palaeoecology: A revision and a test of persistence and discreteness: Geological Society, London, Special Publication 314, no. 1, p. 7–36, https://doi.org/10.1144/SP314.2.

Brett, C.E., Baird, G.C., Bartholomew, A.J., DeSantis, M.K., and Ver Straeten, C.A., 2011, Sequence stratigraphy and a revised sea-level curve for the Middle Devonian of eastern North America: Palaeogeography, Palaeoclimatology, Palaeoecology, v. 304, no. 1–2, p. 21–53, https://doi.org/10.1016/j.palaeo.2010.10.009.

Brocke, R., Fatka, O., Lindemann, R.H., Schindler, E., and Ver Straeten, C.A., 2016, Palynology, dacryoconarids and the lower Eifelian (Middle Devonian) Basal Choteč Event: Case studies from the Prague and Appalachian basins, *in* Becker, R.T., Königshof, P., and Brett, C.E., eds., Devonian Climate, Sea Level and Evolutionary Events: Geological Society, London, Special Publication 423, no. 1, p. 123, https://doi.org/10.1144/SP423.8.

Budil, P., 1995, Demonstrations of the Kačák event (Middle Devonian, uppermost Eifelian) at some Barrandian localities: Vestnik Ceskeho Geologickeho Ustavu, v. 70, no. 4, p. 1–24.

Calvert, S.E., and Pedersen, T.F., 2007, Chapter Fourteen: Elemental proxies for palaeoclimatic and palaeoceanographic variability in marine sediments: Interpretation and application, *in* Claude, H.M., and Anne, D.V., eds., Developments in Marine Geology, Volume 1: Amsterdam, Elsevier, p. 567–644.

Chlupáč, I., and Kukal, Z., 1986, Reflection of possible global Devonian events in the Barrandian area, C.S.S.R, *in* Walliser, O.H., ed., Global Bio-Events. Lecture Notes in Earth Sciences, Volume 8: Berlin, Heidelberg, Springer-Verlag, p. 169–179.

Da Silva, A.C., Hladil, J., Chadimová, L., Slavík, L., Hilgen, F.J., Bábek, O., and Dekkers, M.J., 2016, Refining the Early Devonian time scale using Milankovitch cyclicity in Lochkovian–Pragian sediments (Prague Synform, Czech Republic): Earth and Planetary Science Letters, v. 455, p. 125–139, https://doi.org/10.1016/j.epsl.2016.09.009.

De Vleeschouwer, D., Whalen, M.T., Day, J.E., and Claeys, P., 2012, Cyclostratigraphic calibration of the Frasnian (Late Devonian) time scale (Western Alberta, Canada): Bulletin of the Geological Society of America, v. 124, no. 5–6, p. 928–942, https://doi.org/10.1130/B30547.1.

De Vleeschouwer, D., and Parnell, A.C., 2014, Reducing time-scale uncertainty for the Devonian by integrating astrochronology and bayesian statistics: Geology, v. 42, no. 6, p. 491–494, https://doi.org/10.1130/G35618.1.

De Vleeschouwer, D., Rakociński, M., Racki, G., Bond, D.P.G., Sobień, K., and Claeys, P., 2013, The astronomical rhythm of Late-Devonian climate change (Kowala section, Holy Cross Mountains, Poland): Earth and Planetary Science Letters, v. 365, p. 25–37, https://doi.org/10.1016/j.epsl.2013.01.016.

De Vleeschouwer, D., Boulvain, F., Da Silva, A.-C., Pas, D., Labaye, C., and Claeys, P., 2015, The astronomical calibration of the Givetian (Middle Devonian) timescale (Dinant Synclinorium, Belgium), *in* Da Silva, A.C., Whalen, M.T., Hladil, J., Chadimova, L., Chen, D., Spassov, S., Boulvain, F., and Devleeschouwer, X., eds., Magnetic Susceptibility Application: A Window onto Ancient Environments and Climatic Variations: Geological Society, London, Special Publication 414, p. 245–256, https://doi.org/10.1144/SP414.3.

De Vleeschouwer, D., Da Silva, A.-C., Sinnesael, M., Chen, D., Day, J.E., Whalen, M.T., Guo, Z., and Claeys, P., 2017, Timing and pacing of the Late Devonian mass extinction event regulated by eccentricity and obliquity: Nature Communications, v. 8, no. 2268, https://doi.org/10.1038/s41467-017-02407-1.

Ellwood, B.B., Tomkin, J.H., El Hassani, A., Bultynck, P., Brett, C.E., Schindler, E., Feist, R., and Bartholomew, A.J., 2011, A climate-driven model and development of a floating point time scale for the entire Middle Devonian Givetian Stage: A test using magnetostratigraphy susceptibility as a climate proxy: Palaeogeography, Palaeoclimatology, Palaeoecology, v. 304, no. 1–2, p. 85–95, https://doi.org/10.1016/j.palaeo.2010.10.014.

Ellwood, B.B., El Hassani, A., Tomkin, J.H., and Bultynck, P., 2015, A climate-driven model using time-series analysis of magnetic susceptibility (χ) datasets to represent a floating-point high-resolution geological timescale for the Middle Devonian Eifelian stage, *in* Da Silva, A.C., Whalen, M.T., Hladil, J., Chadimova, L., Chen, D., Spassov, S., Boulvain, F., and Devleeschouwer, X., eds., Magnetic Susceptibility Application: A Window onto Ancient Environments and Climatic Variations: Geological Society, London, Special Publication 414, p. 209, https://doi.org/10.1144/SP414.4.

House, M., 1981, Lower and Middle Devonian goniatite biostratigraphy, *in* Oliver, Jr., W.A., and Klapper, G., eds., Biostratigraphy of New York: Washington, D.C., International Union of Geological Sciences Subcommission on Devonian Stratigraphy, p. 33–38.

House, M.R., 1985, Correlation of mid-Palaeozoic ammonoid evolutionary events with global sedimentary perturbations: Nature, v. 313, no. 5997, p. 17–22, https://doi.org/10.1038/313017a0.

House, M.R., 2002, Strength, timing, setting and cause of mid-Paleozoic extinctions: Palaeogeography, Palaeoclimatology, Palaeoecology, v. 181, no. 1–3, p. 5–25, https://doi.org/10.1016/S0031-0182(01)00471-0.

House, M.R., and Stubblefield, C.J., 1965, A study in the tornoceratidae: The succession of ***tornoceras*** and related genera in the North American Devonian: Philosophical Transactions of the Royal Society of London. Series B, Biological Sciences, v. 250, no. 763, p. 79–130, https://doi.org/10.1098/rstb.1965.0021.

Klapper, G., 1981, Review of New York Devonian conodont biostratigraphy, *in* Oliver, Jr., W.A., and Klapper, G., eds., Devonian Biostratigraphy of New York: Washington, D.C., International Union of Geological Sciences Subcommission on Devonian Stratigraphy, p. 57–66.

Klapper, G., and Ziegler, W., 1979, Devonian conodont biostratigraphy, *in* House, M.R., Scrutton, C.T., and Basset, M.G., eds., The Devonian System: Palaeontological Association Special Paper 23, p. 199–224.

Königshof, P., Da Silva, A.C., Suttner, T.J., Kido, E., Waters, J., Carmichael, S.K., Jansen, U., Pas, D., and Spassov, S., 2016, Shallow-water facies setting around the Kačák Event: A multidisciplinary approach, *in* Becker, R.T., Königshof, P., and Brett, C.E., eds., Devonian Climate, Sea Level, and Evolutionary Events: Geological Society, London, Special Publication 423, p. 171–199, https://doi.org/10.1144/SP423.4.

Laskar, J., Fienga, A., Gastineau, M., and Manche, H., 2011, La2010: A new orbital solution for the long-term motion of the Earth: Astronomy & Astrophysics, v. 532, 15 p., https://doi.org/10.1051/0004-6361/201116836.

Le Hir, G., Donnadieu, Y., Goddéris, Y., Meyer-Berthaud, B., Ramstein, G., and Blakey, R.C., 2011, The climate change caused by the land plant invasion in the Devonian: Earth and Planetary Science Letters, v. 310, no. 3, p. 203–212, https://doi.org/10.1016/j.epsl.2011.08.042.

Martinez, M., Kotov, S., De Vleeschouwer, D., Pas, D., and Pälike, H., 2016, Testing the impact of stratigraphic uncertainty on spectral analyses of sedimentary series: Climate of the Past, v. 12, no. 9, p. 1765–1783, https://doi.org/10.5194/cp-12-1765-2016.

Meyers, S., 2014, Astrochron: An R Package for Astrochronology: http://www.geology.wisc.edu/~smeyers.

Meyers, S.R., and Sageman, B.B., 2007, Quantification of deep-time orbital forcing by average spectral misfit: American Journal of Science, v. 307, no. 5, p. 773–792, https://doi.org/10.2475/05.2007.01.

Muller, R.A., and MacDonald, G.J., 2000, Ice Ages and Astronomical Causes: Data, Spectral Analyses and Mechanisms: Chichester, UK, Springer-Praxis, 318 p.

Niedźwiedzki, G., Szrek, P., Narkiewicz, K., Narkiewicz, M., and Ahlberg, P.E., 2010, Tetrapod trackways from the early Middle Devonian period of Poland: Nature, v. 463, no. 7277, p. 43–48, https://doi.org/10.1038/nature08623.

Olsen, P.E., Grand cycles of the Milankovitch Band [abs.], Eos (Transactions, American Geophysical Union), v. 82 (47), Fall Meeting Supplement.

Pas, D., Hinnov, L., Day, J.E., Kodama, K., Sinnesael, M., and Liu, W., 2018, Cyclostratigraphic calibration of the Famennian stage (Late Devonian, Illinois Basin, USA): Earth and Planetary Science Letters, v. 488, p. 102–114, https://doi.org/10.1016/j.epsl.2018.02.010.

Roden, M.K., Parrish, R.R., and Miller, D.S., 1990, The absolute age of the Eifelian Tioga ash bed, Pennsylvania: The Journal of Geology, v. 98, no. 2, p. 282–285, https://doi.org/10.1086/629399.

Sepkoski, J.J., 1997, Biodiversity: Past, present, and future: Journal of Paleontology, v. 71, no. 4, p. 533–539, https://doi.org/10.1017/S0022336000040026.

Sinnesael, M., Loi, A., Dabard, M.-P., Vandenbroucke, T., and Claeys, P., 2017, Cyclostratigraphic analysis of the Middle to lower Upper Ordovician Postolonnec Formation in the Armorican Massif (France): Integrating pXRF, gamma-ray and lithological data: Proceedings European Geosciences Union General Assembly Conference Abstracts, Volume 19, p. 9565.

Sinnesael, M., De Vleeschouwer, D., Zeeden, C., Batenburg, S.J., Da Silva, A.-C., de Winter, N.J., Dinarès-Turell, J., Drury, A.J., Gambacorta, G., Hilgen, F.J., Hinnov, L.A., Hudson, A.J.L., Kemp, D.B., Lantink, M.L., Laurin, J., Li, M., Liebrand, D., Ma, C., Meyers, S.R., Monkenbusch, J., Montanari, A., Nohl, T., Pälike, H., Pas, D., Ruhl, M., Thibault, N., Vahlenkamp, M., Valero, L., Wouters, S., Wu, H., and Claeys, P., 2019, The Cyclostratigraphy Intercomparison Project (CIP): Consistency, merits and pitfalls: Earth-Science Reviews, v. 199, p. 102965, https://doi.org/10.1016/j.earscirev.2019.102965.

Taner, M., 2000, Attributes Revisited. Technical Publication: Houston, Texas, Rock Solid Images, Inc.

Thomson, D.J., 1982, Spectrum estimation and harmonic analysis: Proceedings of the Institute of Electrical and Electronics Engineers, v. 70, no. 9, p. 1055–1096, https://doi.org/10.1109/PROC.1982.12433.

Tucker, R.D., Bradley, D.C., Ver Straeten, C.A., Harris, A.G., Ebert, J.R., and McCutcheon, S.R., 1998, New U-Pb zircon ages and the duration and division of Devonian time: Earth and Planetary Science Letters, v. 158, no. 3, p. 175–186, https://doi.org/10.1016/S0012-821X(98)00050-8.

Ver Straeten, C.A., 2007, Basinwide stratigraphic synthesis and sequence stratigraphy, upper Pragian, Emsian and Eifelian stages (Lower to Middle Devonian), Appalachian Basin, *in* Becker, R.T., and Kirchgasser, W.T., Devonian Events and Correlations: Geological Society, London, Special Publication 278, no. 1, p. 39–81, https://doi.org/10.1144/SP278.3.

Vodrážková, S., Frýda, J., Suttner, T.J., Koptíková, L., and Tonarová, P., 2013, Environmental changes close to the Lower–Middle Devonian boundary; the Basal Choteč Event in the Prague Basin (Czech Republic): Facies, v. 59, no. 2, p. 425–449, https://doi.org/10.1007/s10347-012-0300-x.

Walliser, O.H., 1986, The IGCP Project 216: Global Biological Events in Earth History, *in* Walliser, O.H., ed., Global Bio-Events. Lecture Notes in Earth Sciences, Volume 8: Berlin, Heidelberg, Springer-Verlag, p. 1–4.

Wu, H., Fang, Q., Wang, X., Hinnov, L.A., Qi, Y., Shen, S.-z., Yang, T.Y., Li, H., Chen, J., and Zhang, S., 2019, An ~34 m.y. astronomical time scale for the uppermost Mississippian through Pennsylvanian of the Carboniferous System of the Paleo-Tethyan realm: Geology, v. 47, no. 1, p. 83–86, https://doi.org/10.1130/G45461.1.

Yao, X., Zhou, Y., and Hinnov, L.A., 2015, Astronomical forcing of a middle Permian chert sequence in Chaohu, South China: Earth and Planetary Science Letters, v. 422, p. 206–221, https://doi.org/10.1016/j.epsl.2015.04.017.

Science Editor: Brad S. Singer
Associate Editor: Bradley Cramer

Manuscript Received 16 December 2019
Revised Manuscript Received 27 March 2020
Manuscript Accepted 5 May 2020

Printed in the USA